American Mineralogist, Volume 60, pages 1092–1097, 1975

High Temperature Crystal Chemistry of Fayalite[1]

JOSEPH R. SMYTH

Lunar Science Institute
3303 NASA Road 1, Houston, Texas 77058

Abstract

The crystal structure of a pure synthetic fayalite has been refined from three dimensional X-ray intensity data measured at 20°, 300°, 600°, and 900°C. Cell dimensions have been determined at 20°, 300°, 450°, 600°, 750°, and 900°C. Comparison of the structures with those of other Mg-Fe olivines is consistent with a slight preference of Fe for the smaller but more distorted $M1$ site. With increasing temperature, the $M1$–O and $M2$–O distances tend to become more regular while the central bond angles of the octahedra show increasing distortion.

Introduction

Being a major constituent of the upper mantle and of basic igneous rocks of the Earth and Moon, the forsterite–fayalite crystalline solution series has been the subject of much recent crystal-chemical investigation. Crystalline solution between the two end-members appears to be very nearly, but not perfectly, ideal (Williams, 1972). Cell dimensions have been found to differ only slightly from linearity between the end members Mg_2SiO_4 and Fe_2SiO_4 (Yoder and Sahama, 1957; Jambor and Smith, 1964; Louisnathan and Smith, 1968; and Fisher and Medaris, 1969). The olivine crystal structure was first determined by Bragg and Brown (1926). Recently there have been several modern refinements of the crystal structures at different compositions, primarily with Fa < 50: Fa_{10}, Fa_{46}, Fa_{50}, Fa_{98} (Birle *et al,* 1968); Fa_{26}, Fa_{51} (Finger, 1970); Fa_{01}, Fa_{40}, Fa_{30}, Fa_{32} (Wenk and Raymond, 1973); Fa_{18}, Fa_{29}, Fa_{31} (Brown and Prewitt, 1973); Fo_{100} and Fa_{60} (Smyth and Hazen, 1973). In these crystal structure studies, Finger, Wenk and Raymond, and Prewitt and Brown have noticed a small but significant preference of Fe for the smaller, but more distorted, $M1$ site, with $M1$ containing two to five percent more iron than $M2$. In these studies the greatest preference of Fe for $M1$ has been found in volcanic specimens while metamorphic olivines tend toward complete disorder. Mössbauer γ-resonance spectroscopy studies (Bush, Hafner, and Virgo, 1970; Virgo and Hafner, 1972) have confirmed a small preference of Fe for one of the two M sites in some olivines. Shinno *et al* (1974) conclude from a Mössbauer study of heated natural olivines that the preference of Fe for $M1$ increases with increasing temperatures and have reported reverse order (more Fe in $M2$) in some low temperature magnesian olivines.

There have also been several studies of the effects of increasing temperatures on the olivine structure. Thermal expansion curves for olivines of several compositions have been determined (Kozu, Ueda, and Tsurumi, 1934; Rigby, Lovell, and Green, 1945, 1946; Skinner, 1962). The olivine structure has recently been refined at elevated temperatures for several compositions: Fo_{100} and Fa_{60} (Smyth and Hazen, 1973); and Fa_{30} (Brown and Prewitt, 1973). Both reports indicate slightly increased order of Fe in $M1$ with increasing temperature. The former authors attributed this to possible oxidation of the sample, while the latter authors noted that it could be accounted for by an increased angular distortions of $M1$ relative to $M2$ with increasing temperature. I have undertaken the study of the crystal structure of a pure synthetic fayalite at elevated temperatures in order to provide a useful point for comparison with other olivine crystal structures.

Intensity Measurement and Structure Refinements

Crystals up to 1 mm in greatest dimension were grown from a pure fayalite melt at 1210°C in a gas-mixing furnace at an oxygen fugacity near the quartz-fayalite-iron buffer. The composition of the crystals was confirmed by microprobe analysis to be pure Fe_2SiO_4 with impurities less than 0.1 percent.

A roughly equant anhedral crystal fragment approximately 150 μm in greatest dimension was selected for study. One-hundred-hour precession

[1] Lunar Science Institute Contribution No. 214.

TABLE 1. Intensity Measurement and Refinement

	20°C	300 C	600 C	900 C
Intensity Measurement				
Radiation	MoKσ	MoKσ	MoKσ	MoKσ
KV/Ma	40/16	40/16	40/16	40/16
2θ Monochromator	11.6°	11.6°	11.6°	11.6°
2θ Scan Speed (°/min)	0.5	1.0	1.0	1.0
Maximum 2θ (°)	75	60	60	60
No. measurements	978	558	570	573
No. observations (I>3σ)	625	359	335	306
Refinement				
No. intensities rejected	4	3	3	2
R	.047	.049	.053	.074
R (wt)	.044	.041	.044	.055

camera exposures on each major axis confirmed the space group as *Pbnm* with no evidence of the super cell reflections reported by Eliseev (1958). The crystal was remounted in an evacuated silica-glass capillary according to the method described by Smyth (1972). Intensity data were measured at 20°, 300°, 600°, and 900°C using a Picker FACS-1 computer-controlled diffractometer. Using the heater described by Smyth (1972) equipped with a feed-back controller, the temperature was maintained to ±5°C at 300° and 600° and to ±15°C at 900°C during intensity measurement. Details of each set of intensity measurements are given in Table 1. Cell dimensions (Table 2) were calculated from a least squares fit to the diffractometer angles obtained by manually centering twelve strong diffraction peaks at 20°, 300°, 450°, 600°, 750°, and 900°C.

All intensities were corrected for Lorentz and polarization effects and for absorption differences using numerical integration techniques (Burnham, 1966). Based on the calculated linear absorption coefficient 96.7 cm^{-1}, transmission factors varied from 0.26 to 0.51. All refinements of the structure models were done with a version of the full-matrix least squares refinement program RFINE (Finger, 1969). All observations were weighted according to $W = 1/\sigma_F^2$ where σ_F is the standard deviation based on counting statistics as described by Burnham *et al* (1971). All observations below the minimum observable level (3σ) were rejected from the normal equations matrix during refinement. Atomic scattering factors used were those given by Cromer and Mann (1968) for half-ionized atoms as derived from Hartree-Fock wave functions neglecting relativistic effects. Real and imaginary anomalous dispersion terms (Cromer and Liberman, 1968) were also in-

TABLE 2. Cell Dimensions of Fayalite

Temperature	a (Å)	b (Å)	c (Å)	Vol. (Å^3)
20°C	4.818(2)	10.471(3)	6.086(2)	307.02(8)
300°C	4.825(1)	10.491(2)	6.100(1)	308.80(7)
450°C	4.836(2)	10.498(3)	6.109(2)	310.12(9)
600°C	4.841(1)	10.521(2)	6.126(1)	311.96(7)
750°C	4.851(2)	10.540(3)	6.139(2)	313.83(9)
900°C	4.860(1)	10.559(2)	6.150(1)	315.64(7)
TEC	9.9 (3)*	9.5 (3)*	11.9 (4)*	3.19 (3)**

* *Mean Linear thermal expansion coefficient 20°-900°C expressed as* $^{o}C^{-1} \times 10^{6}$.

***Mean Volume thermal expansion coefficient 20-900°C expressed as* $^{o}C^{-1} \times 10^{5}$.

TABLE 3. Positional and Thermal Parameters

		20°C	300°C	600°C	900°C
M1	X	0	0	0	0
	Y	0	0	0	0
	Z	0	0	0	0
	β_{11}	0.0035(3)	0.0075(5)	0.0129(6)	0.0190(11)
	β_{22}	0.0019(1)	0.0038(1)	0.0060(1)	0.0079(2)
	β_{33}	0.0035(2)	0.0072(3)	0.0111(4)	0.0199(7)
	β_{12}	0.0002(2)	0.0005(3)	0.0003(4)	0.0004(6)
	β_{13}	-0.0006(3)	-0.0009(5)	-0.0019(6)	-0.0030(10)
	β_{23}	-0.0004(1)	-0.0009(2)	-0.0017(2)	-0.0027(4)
	B eq.	0.57(1)	1.14(4)	1.84(6)	2.78(8)
M2	X	0.9853(2)	0.9859(3)	0.9866(4)	0.9871(6)
	Y	0.2800(1)	0.2803(1)	0.2806(1)	0.2808(2)
	Z	1/4	1/4	1/4	1/4
	β_{11}	0.0045(3)	0.0105(6)	0.0170(8)	0.0249(13)
	β_{22}	0.0013(1)	0.0026(1)	0.0040(1)	0.0051(2)
	β_{33}	0.0034(2)	0.0065(3)	0.0102(5)	0.0159(7)
	β_{12}	0.0000(1)	0.0002(2)	-0.0002(3)	0.0002(6)
	B eq.	0.50(1)	1.03(4)	1.63(6)	2.35(8)
Si	X	0.4292(4)	0.4294(5)	0.4295(6)	0.4288(9)
	Y	0.0975(2)	0.0976(3)	0.0975(3)	0.0971(4)
	Z	1/4	1/4	1/4	1/4
	β_{11}	0.0019(6)	0.0040(9)	0.0066(14)	0.0095(20)
	β_{22}	0.0012(2)	0.0022(2)	0.0034(3)	0.0037(5)
	β_{33}	0.0034(5)	0.0060(8)	0.0077(9)	0.0144(15)
	β_{12}	0.0002(3)	0.0005(4)	0.0001(5)	0.0007(8)
	B eq.	0.41(1)	0.74(8)	1.09(9)	1.57(12)
O1	X	0.7687(10)	0.7672(12)	0.7673(15)	0.7674(23)
	Y	0.0928(5)	0.0933(6)	0.0936(7)	0.0941(11)
	Z	1/4	1/4	1/4	1/4
	β_{11}	0.0026(15)	0.0025(30)	0.0126(35)	0.0138(50)
	β_{22}	0.0014(4)	0.0027(7)	0.0036(9)	0.0050(14)
	β_{33}	0.0049(12)	0.0081(19)	0.0103(24)	0.0156(42)
	β_{12}	0.0014(8)	0.0018(10)	0.0019(15)	0.0029(20)
	B eq.	0.53(2)	0.87(18)	1.44(22)	1.97(30)
O2	X	0.2076(9)	0.2086(10)	0.2094(14)	0.2090(20)
	Y	0.4529(5)	0.4529(6)	0.4527(8)	0.4532(10)
	Z	1/4	1/4	1/4	1/4
	β_{11}	0.0006(15)	0.0038(25)	0.0054(32)	0.0082(49)
	β_{22}	0.0018(4)	0.0033(6)	0.0042(8)	0.0050(12)
	β_{33}	0.0029(10)	0.0054(15)	0.0092(20)	0.0172(35)
	β_{12}	-0.0006(7)	-0.0007(10)	-0.0008(12)	-0.0024(20)
	B eq.	0.42(2)	0.87(15)	1.25(23)	1.87(26)
O3	X	0.2884(7)	0.2897(8)	0.2906(10)	0.2919(14)
	Y	0.1637(3)	0.1630(4)	0.1628(4)	0.1625(6)
	Z	0.0383(6)	0.0395(8)	0.0403(10)	0.0443(13)
	β_{11}	0.0035(12)	0.0072(18)	0.0109(20)	0.0166(35)
	β_{22}	0.0011(3)	0.0020(4)	0.0032(5)	0.0038(8)
	β_{33}	0.0045(9)	0.0079(14)	0.0135(20)	0.0248(30)
	β_{12}	-0.0003(5)	-0.0010(8)	-0.0005(10)	-0.0006(15)
	β_{13}	-0.0005(9)	-0.0015(16)	0.0002(20)	0.0017(32)
	β_{23}	0.0007(4)	0.0011(6)	0.0024(8)	0.0035(14)
	B eq.	0.49(2)	0.91(12)	1.48(16)	2.34(20)

TABLE 4. Magnitude and Orientation of Thermal Vibration Ellipsoids

		M1				M2				Si			
Temperature	axis	RMS Ampl.(Å)	+a	+b	+c	RMS Ampl.(Å)	+a	+b	+c	RMS Ampl.(Å)	+a	+b	+c
20°C	1	0.062(2)	18(6)	90(5)	72(7)	0.072(2)	3(8)	93(7)	90	0.046(2)	6(6)	96(8)	90
	2	0.080(2)	73(6)	108(5)	155(6)	0.080(2)	90	90	180	0.080(3)	90	90	180
	3	0.106(3)	96(6)	162(6)	73(6)	0.086(2)	87(8)	3(8)	90	0.083(4)	84(12)	6(11)	90
300°C	1	0.092(3)	13(8)	93(7)	77(8)	0.111(3)	11(22)	101(24)	90	0.067(3)	9(8)	99(9)	90
	2	0.113(3)	79(7)	112(7)	156(7)	0.111(4)	90	90	180	0.106(3)	90	90	180
	3	0.149(3)	97(8)	158(8)	70(8)	0.120(3)	79(17)	11(19)	90	0.112(4)	81(10)	9(10)	90
600°C	1	0.118(3)	26(9)	85(9)	64(10)	0.140(4)	90	90	0	0.089(3)	1(9)	91(10)	90
	2	0.142(3)	64(9)	111(9)	146(10)	0.142(4)	166(28)	104(24)	90	0.121(3)	90	90	180
	3	0.189(3)	95(10)	158(10)	69(10)	0.150(4)	76(21)	166(22)	90	0.138(4)	89(9)	1(10)	90
900°C	1	0.146(4)	17(12)	86(13)	73(13)	0.170(4)	65(35)	155(33)	90	0.105(4)	10(12)	100(11)	90
	2	0.182(4)	74(11)	126(11)	139(11)	0.173(4)	155(38)	125(39)	90	0.145(4)	100(12)	170(12)	90
	3	0.226(4)	97(12)	144(12)	54(12)	0.175(4)	90	90	0	0.166(4)	90	90	0

		O1				O2				O3			
Temperature	axis	RMS Ampl.(Å)	+a	+b	+c	RMS Ampl.(Å)	+a	+b	+c	RMS Ampl.(Å)	+a	+b	+c
20°C	1	0.033(4)	28(8)	118(8)	90	0.020(4)	9(6)	81(6)	90	0.062(3)	26(18)	65(22)	95(27)
	2	0.096(4)	90	90	180	0.073(4)	90	90	180	0.068(4)	113(16)	43(24)	124(26)
	3	0.100(4)	62(12)	28(14)	90	0.101(4)	81(9)	171(8)	90	0.100(4)	100(9)	58(8)	34(8)
300°C	1	0.037(5)	19(9)	109(8)	90	0.065(6)	7(8)	83(9)	90	0.083(5)	31(12)	59(17)	89(16)
	2	0.123(5)	90	90	180	0.101(6)	90	90	180	0.097(5)	113(14)	47(19)	128(18)
	3	0.128(6)	71(17)	19(19)	90	0.137(5)	83(9)	173(10)	90	0.134(4)	109(10)	58(11)	38(12)
600°C	1	0.110(6)	30(10)	120(9)	90	0.078(7)	6(8)	84(9)	90	0.107(6)	133(19)	129(28)	68(24)
	2	0.140(7)	90	90	180	0.132(7)	90	90	180	0.119(6)	137(22)	55(24)	112(24)
	3	0.153(7)	60(15)	30(18)	90	0.154(8)	84(11)	174(12)	90	0.175(6)	91(11)	58(14)	32(12)
900°c	1	0.114(9)	26(12)	116(11)	90	0.089(9)	17(10)	73(12)	90	0.126(8)	122(28)	142(27)	71(21)
	2	0.173(9)	90	90	180	0.173(9)	107(16)	17(19)	90	0.146(8)	148(26)	69(21)	98(20)
	3	0.179(9)	64(23)	26(21)	90	0.181(9)	90	90	0	0.228(7)	87(21)	70(19)	21(20)

TABLE 6. Metal-Oxygen Distances (Å)*

	20°C	300°C	600°C	900°C
M1 Octahedron				
M1-O1 [2]**	2.121(5)***	2.132(6)	2.141(7)	2.152(11)
M1-O2 [2]	2.131(4)	2.132(5)	2.138(7)	2.147(10)
M1-O3 [2]	2.219(3)	2.222(4)	2.230(5)	2.243(7)
Mean M1-O	2.157	2.162	2.170	2.181
M2 Octahedron				
M2-O1 [1]	2.221(5)	2.229(6)	2.235(7)	2.242(11)
M2-O3 [1]	2.103(3)	2.105(4)	2.108(5)	2.116(7)
M2-O3 [2]	2.080(3)	2.090(4)	2.102(5)	2.129(7)
M2-O3 [2]	2.296(3)	2.305(4)	2.313(5)	2.315(7)
Mean M2-O	2.179	2.187	2.196	2.208
Si Tetrahedron				
Si-O1 [1]	1.636(5)	1.630(6)	1.635(7)	1.646(11)
Si-O2 [1]	1.652(4)	1.658(5)	1.664(7)	1.660(10)
Si-O3 [2]	1.612(3)	1.604(4)	1.605(5)	1.587(7)
Mean Si-O	1.628	1.624	1.627	1.620

* *Distances not corrected for thermal motion.*

** *Figures in brackets are multiplicity of bond in polyhedron.*

*** *Figures in parentheses are the estimated standard deviation in terms of the last decimal place cited.*

TABLE 7. Selected Bond Angles (degrees)

	20°C	300°C	600°C	900°C
M1 Octahedron				
O1-M1-O3 [2]*	84.25(13)**	84.29(16)	84.22(19)	83.81(29)
O1-M1-O3^1 [2]	95.75(13)	95.71(16)	95.78(19)	96.19(29)
O1-M1-O2 [2]	86.63(13)	86.69(16)	86.59(19)	86.59(29)
O1-M1-O2^1 [2]	93.38(13)	93.31(16)	93.41(19)	93.41(29)
O2-M1-O3 [2]	71.92(11)	71.70(13)	71.61(18)	70.85(26)
O2-M1-O3^1 [2]	108.08(11)	108.30(13)	108.39(18)	109.15(26)
Mean O-M1-O	90	90	90	90
σ^2***	135.0	137.6	139.3	151.5
M2 Octahedron				
O1-M2-O3 [2]	80.25(13)	80.26(16)	80.26(19)	80.21(29)
O1-M2-O3^{11} [2]	92.04(13)	92.05(16)	92.01(19)	92.02(29)
O2-M2-O3 [2]	97.63(11)	97.73(13)	97.71(18)	97.95(26)
O2-M2-O3^{111}[2]	89.34(11)	89.25(13)	89.27(18)	89.14(26)
O3-M2-O3^1 [1]	68.22(8)	67.69(10)	67.48(13)	66.26(18)
O3-M2-O3^{11} [2]	88.11(8)	88.23(10)	88.22(13)	88.41(18)
O3-M2-O3^{111}[1]	115.05(8)	115.37(10)	115.60(13)	116.44(18)
Mean O-M2-O	89.83	89.84	89.84	89.85
σ^2	129.5	133.3	135.2	145.0
Si Tetrahedron				
O1-Si-O2 [1]	111.78(13)	112.07(16)	112.42(19)	112.68(29)
O1-Si-O3 [2]	115.71(13)	115.61(16)	115.43(19)	115.30(29)
O2-Si-O3 [2]	103.06(11)	102.88(13)	102.87(18)	103.23(26)
O3-Si-O3^1 [1]	106.04(8)	106.29(10)	106.36(13)	105.71(18)
Mean O-Si-O	109.23	109.22	109.23	109.24

* *Figures in brackets are multiplicity of angle in polyhedron.*

** *Figures in parentheses are the estimated standard deviation in terms of the last decimal place cited.*

*** *Octahedral angle variance* $\sigma_\theta^2 = \sum_{i=1}^{12} \frac{(\theta_i - 90°)^2}{12}$ *(Robinson et al., 1971).*

cluded in each cycle of refinement. The initial model used for the refinement of the room temperature structures was that given for fayalite (Fa_{98}) by Birle *et al* (1968). The structure models at each elevated

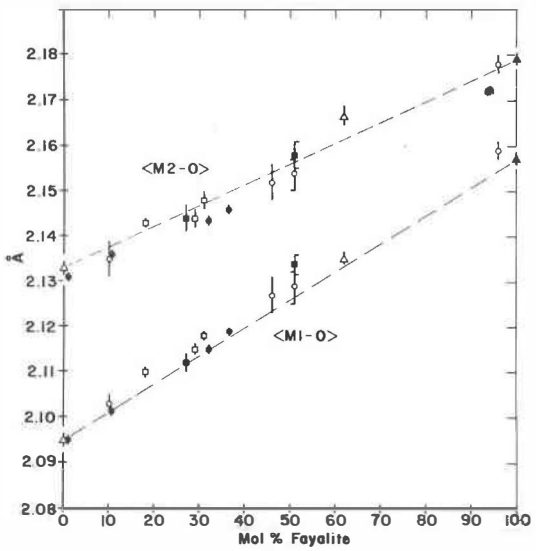

FIG. 1. A plot of the mean $M1$–O and $M2$–O distances versus bulk composition for several modern refinements of the olivine structure at 20°C. Symbols: open circle, Birle *et al* (1968); solid circle, Wenk and Raymond (1972); open square, Brown and Prewitt (1973); solid square, Finger (1970); open triangle, Smyth and Hazen (1973); and solid triangle, this work. The broken lines indicate the strictly linear trend between the end points.

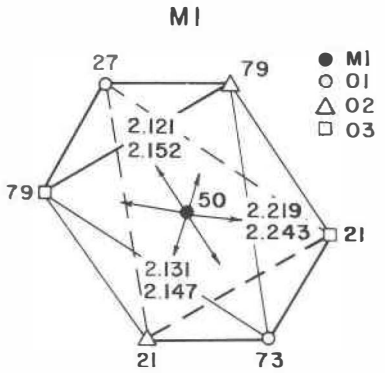

FIG. 2A. An *a*-axis projection of the $M1$ coordination polyhedron (site symmetry $\bar{1}$) showing the $M1$–O distances at 200°C (upper) and 900°C (lower).

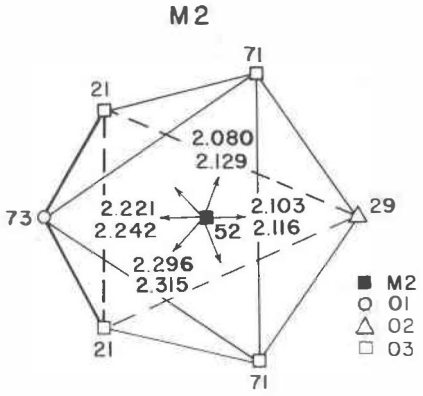

FIG. 2B. An *a*-axis projection of the $M2$ coordination polyhedron (site symmetry m) showing the $M2$–O distances at 20°C (upper figure) and 900°C (lower figure).

temperature were then each refined in turn from the model obtained at the next lower temperature. Final weighted and unweighted R factors are presented in Table 1. Final positional and thermal parameters are presented in Table 3. The magnitudes and orientations of thermal vibration ellipsoids are given in Table 4. The final observed and calculated structure factors are available as Table 5.[2]

Discussion

Cation-oxygen distances are presented in Table 6 and oxygen–cation–oxygen angles are presented in Table 7. Comparison of the room temperature fayalite structure with those of previously determined olivines reveals some aspects of the forsterite-fayalite crystalline solution series. Figure 1 is a plot of the mean $M1$–O and $M2$–O distances as a function of composition. The $M2$–O distances exhibit a nearly linear relationship; however, there is considerable scatter in the intermediate olivines most likely due to variable small amounts of Ca, which should show a strong preference for $M2$. The smaller amount of scatter shown by the $M1$–O distances reveals a slight concave downward curvature. This curvature is most likely due to the preference of Fe for the smaller, but more distorted $M1$ site reported by several workers (Bush *et al*, 1970; Finger, 1970; Finger and Virgo, 1971; Virgo and Hafner, 1972; Wenk and Raymond, 1972). Such curvature indicates that a small preference of Fe in $M1$ is common. A few more refinements of synthetic olivine structures in the composition range Fa_{60-90} would help to confirm this trend.

Figures 2A and 2B are *a* axis projections of $M1$ and $M2$ coordination polyhedra showing the M–O distances at 20° and 900°C. This figure illustrates that there is a slight tendency for the $M2$–O distances to become more regular with increasing temperature. Figure 3 contains plots of several structural

[2] To obtain a copy of Table 5, order Document No. AM-75-009 from the Business Office, Mineralogical Society of America, 1909 K Street, N. W., Washington, D. C. 20006. Please remit $1.00 for the microfiche.

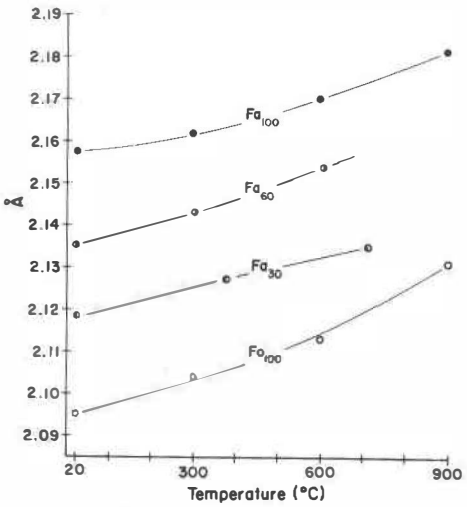

FIG. 3A. A plot of the mean $M1$–O distances versus temperature for several olivines. Fo_{100} and Fa_{60} are from Smyth and Hazen (1973) and Fa_{30} from Brown and Prewitt (1973).

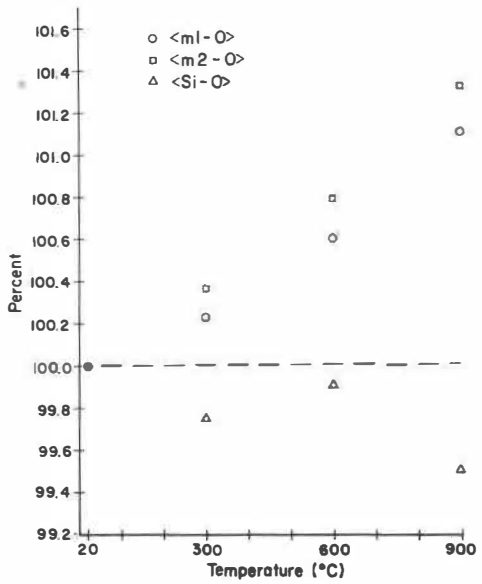

FIG. 3C. A plot of the percent expansion of the mean $M1$–O, $M2$–O, and Si–O distances versus temperature for fayalite.

parameters of olivines as a function of temperature. Figures 3A and 3B are plots of the mean $M1$–O and $M2$–O distances respectively for fayalite and the olivine structures (Fo_{100}, Fa_{30}, and Fa_{61}) previously studied at high temperatures. The smaller M sites of forsterite show slightly greater expansion than the correspondingly larger M sites of fayalite. Fa_{30} and Fa_{60} values show predictable intermediate trends indicating that the near ideality of forsterite–fayalite solid solutions extends to elevated temperatures. Figure 3C is a plot of the relative expansions of the mean $M1$–O, $M2$–O, and SiO distances. As has been noted in previous high temperature crystallographic studies of ferromagnesian silicates (Smyth, 1971, 1973, 1974; Brown and Prewitt, 1973; Smyth and Hazen, 1973; Cameron *et al.*, 1973), the M–O distances show large positive expansions while the Si–O distances show zero or slightly negative expansions. Figure 3D is a plot of the octahedral angle variance which Robinson *et al* (1971) defined as a sensitive

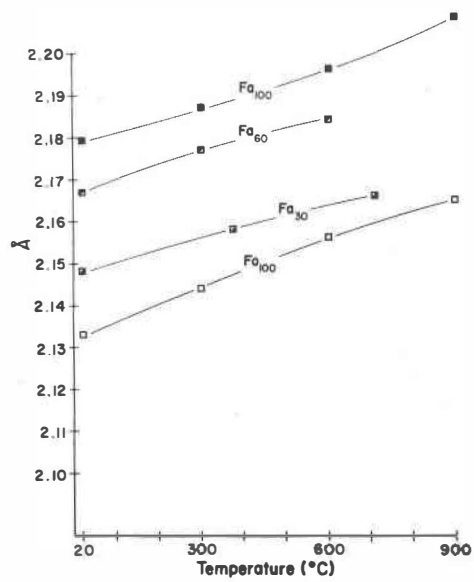

FIG. 3B. A plot of the mean $M2$–O distances versus temperatures for several olivines. References are the same as for Figure 2A.

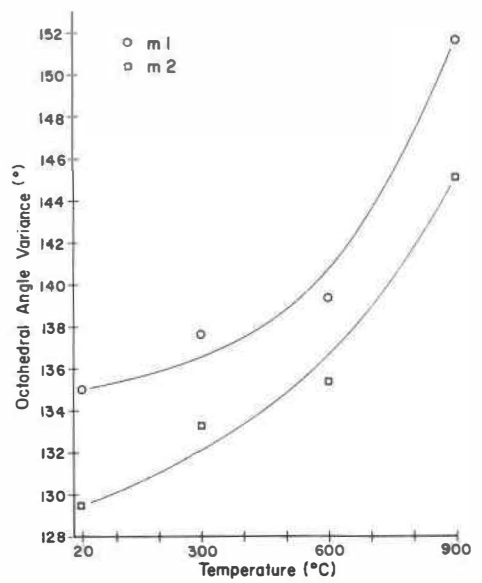

FIG. 3D. A plot of the octahedral angle variance (as defined by Robinson *et al*, 1971) versus temperature for fayalite.

measure of angular distortion in octahedral coordination polyhedra. The curves for fayalite are similar to those of Brown and Prewitt (1973) and show sharply increasing angular distortion of the $M1$ and $M2$ octahedra above 600°C.

Conclusions

The refinement of the room temperature structure of a pure fayalite has provided a useful point of comparison for the review of the iron-magnesium olivine structures. The high temperature structure refinements have shown that fayalite behaves like forsterite with increasing temperature and thus there are no radical changes in the structures up to 900°C. They have shown that with increasing temperature, the $M1$–O and $M2$–O distances tend to become slightly more regular while the octahedral angles show increasing distortion.

Acknowledgments

The author thanks Dr. T. M. Usselman for synthesizing the sample and for microprobe chemical analysis. This study was supported by the Lunar Science Institute which is operated by the Universities Space Research Association under contract No. NSR 09-051-001 with the National Aeronautics and Space Administration. This paper constitutes Lunar Science Institute Contribution No. 214.

References

Birle, J. D., G. V. Gibbs, P. B. Moore, and J. V. Smith (1968) Crystal structures of natural olivines. *Am. Mineral.* **53,** 807–824.

Bragg, W. L., and G. B. Brown (1926) Die Struktur des Olivins. *Z. Kristallogr.* **63,** 538–556.

Brown, G. E., and C. T. Prewitt (1973) High temperature crystal chemistry of hortonolite. *Am. Mineral.* **58,** 577–587.

Burnham, C. W. (1966) Computation of absorption correction and significance of end effect. *Am. Mineral.* **51,** 159–167.

———, Y. Ohashi, S. S. Hafner, and D. Virgo (1971) Cation distribution and atomic thermal vibrations in an iron-rich orthopyroxene. *Am. Mineral.* **56,** 850–876.

Bush, W. R., S. S. Hafner, and D. Virgo (1970) Some ordering of iron and magnesium at the octahedrally coordinated sites in a magnesium-rich olivine. *Nature,* **227,** 1339–1341.

Cameron, M., S. Sueno, C. T. Prewitt, and J. J. Papike (1973) High temperature crystal chemistry of acmite, diopside, hedenbergite, jadeite, spodumene, and ureyite. *Am. Mineral.* **58,** 594–618.

Cromer, D. T., and D. Liberman (1968) Relativistic calculation of anomalous scattering factors for X-rays. *J. Chem. Phys.* **53,** 1891–1898.

———, and J. B. Mann (1968) X-ray scattering factors computed from numerical Hartree-Fock wave functions. *Acta Crystallogr.* **24,** 321–324.

Eliseev, E. N. (1958) New data on the crystal structure of olivine. *Kristallografiya,* **3,** 167–175 (Russian); *Sov. Phys. Crystallogr.* **3,** 163–170.

Finger, L. W. (1969) Determination of cation distribution by least squares refinement of single crystal X-ray data. *Carnegie Inst. Washington Year Book,* **67,** 216–217.

——— (1970) Fe/Mg ordering in olivines. *Carnegie Inst. Washington Year Book,* **69,** 302–305.

———, and D. Virgo (1971) Confirmation of Fe/Mg ordering in olivines. *Carnegie Inst. Washington Year Book,* **70,** 221–225.

Fisher, G. W., and L. G. Medaris (1969) Cell dimensions and X-ray determinative curve for synthetic Mg-Fe^{2+} olivines. *Am. Mineral.* **54,** 741–753.

Jambor, J. L., and J. V. Smith (1964) Olivine composition determination with small diameter X-ray powder cameras. *Mineral. Mag.* **33,** 730–741.

Kozu, S., J. Ueda, and S. Tsurumi (1934) Thermal expansion of olivine. *Proc. Imp. Acad. Japan,* **10,** 83–86.

Louisnathan, S. J., and J. V. Smith (1968) Cell dimensions of olivine. *Mineral. Mag.* **36,** 1123–1134.

Rigby, G. R., G. B. H. Lovell, and A. T. Green (1945) The reversible thermal expansion and other properties of some calcium ferrous silicates. *Trans. Br. Ceram. Soc.* **44,** 37–52.

———, ———, and ——— (1946) The reversible thermal expansion and other properties of some magnesian ferrous silicates. *Trans. Br. Ceram. Soc.* **45,** 237–250.

Robinson, K., G. V. Gibbs, and P. H. Ribbe (1971) Quadratic elongation: a quantitative measure of distortion in coordination polyhedra. *Science,* **172,** 567–570.

Shinno, I., M. Hayashi, and Y. Kuroda (1974) Mössbauer study of natural olivines. *Mineral. J. (Japan),* **7,** 344–358.

Skinner, B. J. (1962) Thermal expansion of ten minerals. *U. S. Geol. Surv. Prof. Pap.* **450D,** 109–112.

Smyth, J. R. (1971) Protoenstatite: a crystal structure refinement at 1100°C. *Z. Kristallogr.* **134,** 262–272.

——— (1972) A simple heating stage for single-crystal diffraction studies up to 1000°C. *Am. Mineral.* **57,** 1305–1309.

——— (1973) An orthopyroxene structure up to 850°C. *Am. Mineral.* **58,** 636–648.

——— (1974) The high temperature crystal chemistry of clinohypersthene. *Am. Mineral.* **59,** 1069–1082.

———, and R. M. Hazen (1973) The crystal structures of forsterite and hortonolite at several temperatures up to 900°C. *Am. Mineral.* **58,** 588–593.

Virgo, D., and S. S. Hafner (1972) Temperature-dependent Mg,Fe distribution in a lunar olivine. *Earth. Planet. Sci. Lett.* **14,** 305–312.

Wenk, H.-R., and K. N. Raymond (1972) Four new structure refinements of olivine. *Z. Kristallogr.* **137,** 86–105.

Williams, R. J. (1972) Activity-composition relations in the fayalite-forsterite solid solution series between 900°C and 1300°C at low pressures. *Earth Planet. Sci. Lett.* **15,** 296–300.

Yoder, H. S., Jr., and T. G. Sahama (1957) Olivine X-ray determinative curve. *Am. Mineral.* **42,** 475–491.

Manuscript received, February 14, 1975; accepted for publication, July 11, 1975.